

Thermodynamic Measurements of Fe-Rh Alloys

David W. Cooke* and F. Hellman

*Department of Physics, University of California at Berkeley, Berkeley, California 94720-7300, USA
Materials Science Division, Lawrence Berkeley National Laboratory, Berkeley, California 94720, USA*

C. Baldasseroni

Department of Materials Science and Engineering, University of California at Berkeley, Berkeley, California 94720-1760, USA

C. Bordel

*Department of Physics, University of California at Berkeley, Berkeley, California 94720-7300, USA and GPM, UMR CNRS 6634,
Université de Rouen, Avenue de l'Université—BP12, 76801 St Etienne du Rouvray, France*

S. Moyerman and E. E. Fullerton

*Center for Magnetic Recording Research, University of California at San Diego, La Jolla, California 92093-0401, USA
(Received 21 April 2012; published 18 December 2012)*

FeRh undergoes an unusual antiferromagnetic-to-ferromagnetic (AFM-FM) transition just above room temperature ($T_{\text{AFM}>\text{FM}}$) that can be tuned or even completely suppressed with small changes in composition. The underlying temperature-dependent entropy difference between the competing AFM and FM states that drives this transition is measured by specific heat as a function of temperature from 2 to 380 K on two nearly equiatomic epitaxial Fe-Rh films, one with a ferromagnetic ground state (Fe-rich) and the other with an antiferromagnetic ground state (Rh-rich). The FM state shows an excess heat capacity near 100 K associated with magnetic excitations that are not present in the AFM state. The integrated entropy and enthalpy differences between the two alloys up to $T_{\text{AFM}>\text{FM}}$ agree with the previously measured entropy of the transition ($\Delta S = 17 \pm 3 \text{ J/kg/K}$) and yield a $T = 0$ energy difference of 3.4 J/g, consistent with literature calculations and experimental data; this agreement supports the use of the Fe-rich FM sample as a proxy for the (unstable) FM state of the AFM Rh-rich sample. From the low-temperature specific heat, along with sound velocity and photoemission measurements, the lattice contribution to the difference ($\Delta S_{\text{latt}} = -33 \pm 9 \text{ J/kg/K}$) and electronic contribution ($\Delta S_{\text{el}} = 8 \pm 1 \text{ J/kg/K}$) to the difference in entropy are calculated, from which the excess heat capacity in the FM phase and the resulting entropy difference are shown to be dominated by magnetic fluctuations ($\Delta S_{\text{mag}} = 43 \pm 9 \text{ J/kg/K}$). The excess magnetic heat capacity is dominated by the magnetic heat capacity of the FM phase, which can be fit to a Schottky-like anomaly with an energy splitting of $16 \pm 1 \text{ meV}$ and a multiplicity of 1 per unit cell.

DOI: [10.1103/PhysRevLett.109.255901](https://doi.org/10.1103/PhysRevLett.109.255901)

PACS numbers: 65.40.Ba, 71.20.Be

Introduction.—In today's information age, information density is at a premium. However, as the bit size becomes smaller and smaller, traditional media runs into the superparamagnetic limit as the anisotropy energy becomes comparable to $k_B T$, leading to thermal instability of bits and/or the difficulty of writing bits in accessible magnetic fields. Thus, denser storage mandates new approaches such as perpendicular media and thermally assisted magnetic recording. One novel approach to thermally assisted magnetic recording involves an FePt and FeRh bilayer, utilizing the unique antiferromagnetic-to-ferromagnetic (AFM-FM) transition of FeRh to improve the writing process of the highly anisotropic perpendicular FePt layer [1].

This unusual AFM > FM transition in FeRh was discovered about 70 years ago [2]. It is known to be first order, with a latent heat of 2.2 kJ/kg [3], a $\sim 1\%$ volume change, and a magnetic-field—dependent transition temperature $T_{\text{AFM}>\text{FM}}$. There remain basic questions about what drives

this transition. The earliest models suggested that the transition was driven by exchange inversion, in which thermal expansion causes a change in the sign of the exchange interaction, but this model was inconsistent with the large entropy change at the transition and other issues discussed by several authors [4,5]. Early low-temperature specific heat $C(T)$ measurements on binary and ternary alloys near the equiatomic FeRh composition showed a substantial reduction in the Sommerfeld coefficient γ [proportional to the electronic density of states (DOS)] for alloys with an AFM ground state compared to those with a FM ground state. Based on this data, Tu *et al.* suggested that an electronic entropy difference drives the transition [6]. First-principle calculations later agreed with the large ground state electronic DOS difference [7]. However, this model is contradicted by specific heat results on Fe-Rh-Ir alloys that show an inverse relationship in γ [8]. More recent models focus on magnetic fluctuations

and on the nature of the Rh moment in each state. Gruner *et al.* evaluate FeRh in an Ising model, explaining the transition through entropy associated with competing magnetic states of the Rh atom [9]. Their model yields a Schottky-like anomaly in $C(T)$ at ~ 200 K in the FM state. Another model, by Gu and Antropov, proposes instead that the driving force of the transition is associated with magnon excitations that have higher $C(T)$ and hence higher entropy in the FM phase compared to the AFM phase [10]. This work predicts a peak in the difference between the heat capacity of the FM and AFM phases at moderate temperatures (~ 300 K). Finally, a recent article by Sandratskii and Mavropoulos suggests that noncollinear magnetic excitations coupled with strong Fe-Rh hybridization are important to understanding the magnetism of the AFM state and from there the source of the transition [11]. The specific heat and entropy of FM and AFM states has not been simulated in this model, but recent time-resolved x-ray diffraction (XRD) measurements support this model of the metamagnetic transition [12].

While low-temperature specific heat measurements have been made on bulk alloys of FeRh and related alloys [6,13], both FM and AFM, and high-temperature measurements around the transition itself in AFM FeRh [3], to date no one has measured the specific heat of AFM and FM FeRh alloys in the moderate temperature range where the heat capacity differences in the proposed models are predicted to occur. We have used ion-beam-assist-deposited (IBAD) MgO microcalorimeters [14] to measure the specific heat $C(T)$ of two near-equiatomic epitaxial Fe-Rh films, one with an antiferromagnetic ground state ($\text{Fe}_{0.98}\text{Rh}_{1.02}$) and one with a ferromagnetic ground state ($\text{Fe}_{1.04}\text{Rh}_{0.96}$). Magnetization measurements on the AFM $\text{Fe}_{0.98}\text{Rh}_{1.02}$ sample show it undergoes the AFM $>$ FM transition at 328 K [15]. These two samples have virtually identical properties in their FM states above 328 K, and we therefore use the specific heat of the Fe-rich FM sample as the proxy for the (unstable) low temperature FM phase of FeRh. We observe excess specific heat in the FM state above that of the AFM state at moderate temperatures, which cannot be explained by lattice or electronic contributions, suggesting that magnetic fluctuation models are correct, although the excess $C(T)$ occurs at lower temperatures than predicted by existing models.

Experimental details.—Thermal relaxation calorimetry is a widely used technique for measuring heat capacity of small samples. In Bachmann’s pioneering design [16], the sample is thermally and physically bound to a silicon bolometer consisting of heater, thermometer, and sapphire sample platform that is weakly linked via thin gold wires to a sample block held at temperature T_0 [16]. Our microcalorimeters and more recently nanocalorimeters modify this design by using an amorphous silicon nitride membrane as the sample platform to support and isolate the sample from the silicon frame [17,18]. Amorphous NbSi and Pt thermometers are located on the sample area with matching thermometers on the silicon frame connected

with Pt leads; a differential bridge is used to measure ΔT . Because the transition in FeRh is sensitive to disorder, including polycrystallinity that would result from growth directly on the membrane, we used recently developed IBAD MgO calorimeters (with biaxially ordered MgO underlayer deposited on the nitride membrane)[14] to enable heat capacity measurements of epitaxial Fe-Rh films.

The Fe-Rh films were grown by magnetron sputtering and are nominally 200 nm thick. The AFM $>$ FM $\text{Fe}_{0.98}\text{Rh}_{1.02}$ film (referred to below as AFM, after its ground state) was deposited from an equiatomic FeRh target, while the ferromagnetic film was co-sputtered from this FeRh target and a second (partially masked) Fe target. Both films were grown at 573 K and then annealed for two hours at 873 K. The composition and atomic number density of the films were determined via Rutherford backscattering measurements. The films’ epitaxy was confirmed via four-circle XRD for samples grown on (001) IBAD MgO and neighboring MgO substrates. Fe-Rh films grow (001) out of plane, rotated 45° in plane relative to the MgO to accommodate $\sqrt{2}$ difference in lattice constant. The in-plane order was characterized by setting the polar angle $\psi = 45^\circ$ and measuring the (101) XRD peaks ($\text{Fe}_{0.98}\text{Rh}_{1.02}$: $a = b = 3.005 \text{ \AA}$, $c = 2.959 \text{ \AA}$ (at room temperature; above the AFM $>$ FM transition temperature, $a = b$ is constrained in plane while c is increased by 1%); $\text{Fe}_{1.04}\text{Rh}_{0.96}$: $a = b = 3.006 \text{ \AA}$, $c = 2.961 \text{ \AA}$). The metamagnetic transition was observed in temperature-dependent XRD (see Supplemental Material [19]) and confirmed via SQUID measurements. Further discussion of the film quality of the films and the IBAD MgO substrate is found elsewhere [14].

Results.—Figure 1 depicts $C(T)$ data for the FM $\text{Fe}_{1.04}\text{Rh}_{0.96}$ and AFM $\text{Fe}_{0.98}\text{Rh}_{0.96}$ Fe-Rh films grown on IBAD MgO microcalorimeters. The AFM data match literature results on $\text{Fe}_{0.98}\text{Rh}_{1.02}$, also shown [3]. The data for the FM alloy align with the data on the AFM sample above its transition, signifying that it is an appropriate proxy for the FM phase of FeRh. Note that there is a noticeable (albeit small) excess heat capacity in the FM film at approximately 100 K—this will be discussed below. Field-dependent measurements below $T_{\text{AFM}>\text{FM}}$ were carried out for both films at $H = 0, 4,$ and 8 T but are not shown because they yielded no difference to within error of the measurement technique.

The specific heat of the Fe-Rh alloys can be broken down into electronic, lattice, and magnetic contributions. The low temperature data, shown in the inset to Fig. 1 as C/T vs T^2 , are used to determine the first two from $C/T = \gamma + \beta T^2$. As has been previously found, γ for the FM alloy is significantly larger than γ for the AFM alloy: $\gamma_{\text{FM}} = 8.3 \pm 0.5 \text{ mJ/mol/K}^2 = 53 \pm 3 \text{ } \mu\text{J/g/K}^2$ (slightly smaller than the previously reported range of $59\text{--}66 \text{ } \mu\text{J/g/K}^2$ [6,8]), whereas $\gamma_{\text{AFM}} = 3.5 \pm 0.4 \text{ mJ/mol/K}^2 = 22 \pm 2 \text{ } \mu\text{J/g/K}^2$ (similar to previous measurements of $10\text{--}32 \text{ } \mu\text{J/mol/K}^2$ [6,8]) [20]. The lattice

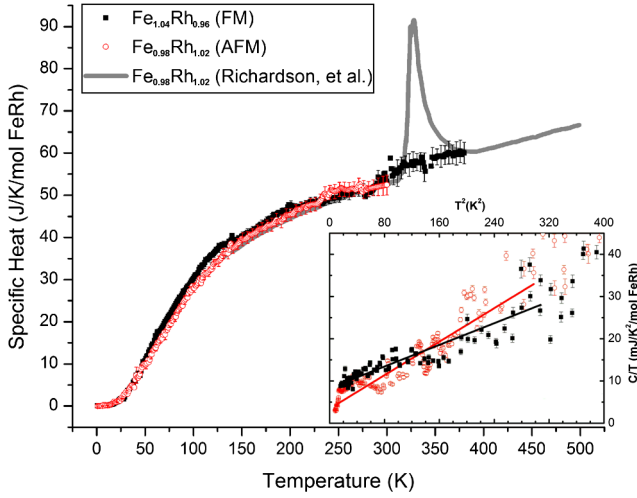


FIG. 1 (color online). Specific heat data for $\text{Fe}_{1.04}\text{Rh}_{0.96}$ (filled black squares) and $\text{Fe}_{0.98}\text{Rh}_{1.02}$ (open red circles) overlaid with data on $\text{Fe}_{0.98}\text{Rh}_{1.02}$ from the literature from 100 to 500 K (gray line) [3]. The inset shows the data for the two Fe-Rh alloys as a function of C/T vs T^2 . The solid black line through the black squares in the inset is a fit to the $\text{Fe}_{1.04}\text{Rh}_{0.96}$ (FM) data with $\gamma = 8.3 \pm 0.5$ mJ/mol/K² and $\Theta_D = 393 \pm 20$ K. The solid red line through the red open circles in the inset is a fit to the $\text{Fe}_{0.98}\text{Rh}_{1.02}$ (AFM) data with $\gamma = 3.5 \pm 0.4$ mJ/mol/K² and $\Theta_D = 340 \pm 13$ K.

contribution is derived from the slope in the low T data. The FM sample exhibits a Debye temperature ($\Theta_D = 393 \pm 20$ K) similar to that seen previously for Fe-Rh alloys near the equiatomic composition [11]. The AFM Debye temperature ($\Theta_D = 340 \pm 13$ K) is somewhat less than the literature value of 390–410 K [4,13], but softening of the AFM compared to FM samples is consistent with literature measurements of the shear modulus G for each [4]. Longitudinal sound velocities v_L were also measured on these films using an ultrasonic picosecond technique [21] and are shown in Table I; they also show the AFM film as softer than the FM. By combining the longitudinal sound velocities with the low-temperature specific heat results, we obtain Θ_D values for the transverse (T) and longitudinal (L) modes of both films as well as the transverse sound velocities, v_T (Table I).

The specific heat data shown in Fig. 1 are taken at constant pressure and hence yield C_P ; theoretical

calculations are commonly done at constant volume. The difference, called the dilation contribution, $C_P - C_V = VT\alpha^2 K_T$ (where $V =$ unit cell volume, α is the volumetric coefficient of thermal expansion, and K_T is the bulk modulus) is small ($< 2\%$ of C) but nonzero near 300 K. The (small) dilation contribution is rewritten as $C_P - C_V = AC_P^2 T$, where $A = VT\alpha^2 K_T / C_P^2$ has been empirically found to be approximately constant with T , so that a determination of A at, e.g., 300 K allows an estimate of dilation at all T [23]. We used temperature-dependent XRD above room temperature to measure α below and above the transition temperature of the $\text{Fe}_{0.98}\text{Rh}_{1.02}$ film, yielding values for both the AFM and FM phases. We calculated the bulk modulus K_T at room temperature from the sound velocities v_L and v_T , which allowed us to calculate $C_V(T)$ for both films. Calculated values of K_T , Young's modulus E , and Poisson ratio ν (see Ref. [4] for methodology) are in good agreement with those calculated or measured previously in the bulk [4,24], giving confidence in these calculations and $C_V(T)$. This calculation of the dilation contribution takes account of most of the anharmonic contribution to the specific heat, leaving a smaller contribution due to what might be called true anharmonicity, which is typically linear to first order and small, hence indistinguishable, from electronic terms.

By subtracting the dilation, lattice, and electronic contributions to the specific heat, we obtain the magnetic contribution. Photoemission data on these same films confirms a low electronic DOS that persists all the way up to the transition [25], with a measurable change at the transition, so we take the electronic contribution to the entropy as simply γT . We treat the lattice contribution in the Debye approximation. The resulting magnetic heat capacity $C_{\text{mag}}(T)$ for each phase is then given by

$$C_{\text{mag}} = C_V - \gamma T - 12R \left(\frac{T}{\Theta_{D,T}} \right)^3 \int_0^{\Theta_{D,T}/T} dx \frac{x^4 e^x}{(e^x - 1)^2} - 6R \left(\frac{T}{\Theta_{D,L}} \right)^3 \int_0^{\Theta_{D,L}/T} dx \frac{x^4 e^x}{(e^x - 1)^2}$$

and is plotted in Fig. 2, with the inset showing $C_{\text{mag}}(T)$ for both the AFM and FM samples and the main figure showing the ΔC_{mag} difference between these. The AFM phase exhibits a small, monotonically increasing $C_{\text{mag}}(T)$, as

TABLE I. v_L = longitudinal sound velocity measured at room temperature; α = volumetric coefficient of thermal expansion, measured from XRD 300–450 K; v_T = transverse sound velocity, E = Young's modulus, ν = Poisson's ratio, and K_T = bulk modulus, calculated from measured low T specific heat Θ_D and v_L . Literature values were based on measured E and assumed ν . Measured values in bold, calculated values in plain font, assumed values in parentheses. α_{FM} measured on $\text{Fe}_{0.98}\text{Rh}_{1.02}$ sample above $T_{\text{AFM} > \text{FM}}$; all other FM values measured on $\text{Fe}_{1.04}\text{Rh}_{0.96}$ sample.

	Θ_D K	$\Theta_{D,L}$ K	$\Theta_{D,T}$ K	v_L km/s	v_T km/s	$\alpha \times 10^5$ /K	E GN/m ²	ν	K_T GN/m ²
FM Fe-Rh(expt.)	393 ± 20	615 ± 12	354 ± 23	4.9 ± 0.1	2.8 ± 0.1	1.75 ± 0.05	197 ± 25	0.25 ± 0.01	133 ± 20
AFM Fe-Rh(expt.)	340 ± 13	591 ± 16	304 ± 21	4.7 ± 0.1	2.4 ± 0.1	2.45 ± 0.09	153 ± 14	0.32 ± 0.01	142 ± 14
FM Fe-Rh(lit.) [4,22]	...	636	338	5.08	2.71	0.8–1.1	190	(0.3)	158
AFM Fe-Rh(lit.) [4,22]	...	603	322	4.80	2.56	1.9	170	(0.3)	142

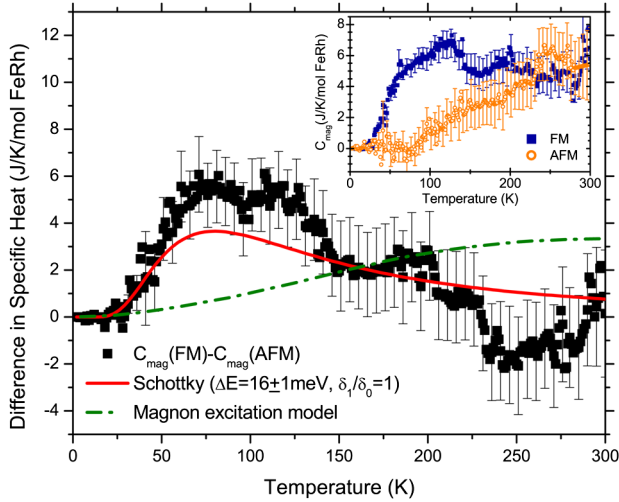


FIG. 2 (color online). Difference in magnetic specific heat data between $\text{Fe}_{1.04}\text{Rh}_{0.96}$ and $\text{Fe}_{0.98}\text{Rh}_{1.02}$. The data is fit to a Schottky two-state anomaly, resulting in an energy splitting of 16 ± 1 meV (solid red line). The excess heat capacity predicted by Gu and Antropov’s magnon fluctuation model [10] is shown for reference (green dashed-dotted line). (inset) Specific heat as a function of temperature for AFM and FM states after subtraction of electronic and lattice contributions.

expected for an AFM material far below its estimated critical temperature ($T_N \approx 840$ K [4]), while the FM phase shows a large peak at ~ 100 K, made even more visible by taking the difference between the two.

Discussion.—Figures 1 and 2 show a difference in the specific heat of the AFM and FM phases. We can thus calculate the entropy difference between these two phases at any temperature, including the phase transition [26]. Integrating this entropy difference from 0 to 300 K should yield the same change in entropy, ΔS , as that measured *via* the latent heat at the AFM \rightarrow FM transition on a single film assuming the FM sample data can be taken as a proxy for the nonequilibrium low- T FM state of the AFM sample. This integration of $\Delta C(T)/T$ yields $\Delta S = 17 \pm 3$ J/kg/K (2.7 ± 0.5 J/mol/K), within the range of 12.6–18.3 J/kg/K, measured previously using the Clausius-Clapeyron relationship [4,27,28], supporting the use of the FM thin film sample as a proxy for the FM phase of the AFM sample. Furthermore, the integration of ΔC gives the enthalpy difference 1.7 ± 0.9 J/g (270 ± 140 J/mol); combined with the calculated latent heat for this sample $L = T\Delta S = 5.1 \pm 0.9$ J/g (810 ± 140 J/mol), which itself is comparable to previous literature values of 5.35 J/g [3,24], this gives a calculated zero temperature energy difference between FM and AFM phases of 3.4 J/g (540 J/mol), consistent with calculations in, e.g., Ref. [10] (0.206 mRyd/atom).

Considering the electronic, lattice, and magnetic contributions, separated as described above, we find $\Delta S_{\text{latt}} = -33 \pm 9$ J/kg/K (5.2 ± 1.4 J/mol/K), $\Delta S_{\text{el}} = 8 \pm 1$ J/kg/K (1.3 ± 0.2 J/mol/K), and $\Delta S_{\text{mag}} = 43 \pm 9$ J/kg/K (6.7 ± 1.4 J/mol/K) (a plot of S_{mag} vs T

can be found in the Supplemental Material [19]). The negative sign on the lattice contribution is notable: because the FM lattice is “stiffer,” it acts to resist the transition and contributes negatively to the entropy of the AFM \rightarrow FM transition, in conflict with earlier models of the AFM \rightarrow FM transition [6,28] but consistent with the calculation of Ricodeau and Melville [4] based on Young’s modulus measurements [5]. The electronic entropy difference does contribute to the transition, as previously observed, but is a much smaller contribution than the magnetic part.

Turning to the temperature dependence of the magnetic contribution to the heat capacity, the most obvious and anomalous signature is the excess heat capacity of the FM phase, which has a peak near 100 K (visible both in $C_{\text{mag}}(T)$ for the FM phase and in the raw $C(T)$ data of Fig. 1, where the FM sample has a significant excess above the AFM sample near 100 K). While the error bars are large, the excess heat capacity of the FM phase above that of the AFM phase can be fit to a Schottky anomaly with an energy splitting $E = 16 \pm 1$ meV shown in Fig. 2; in this fit, we took the multiplicity of the two states to be equal and equal to the number of unit cells (= number of Rh atoms).

In the thermal fluctuation model of Gruner *et al.*, there is a Schottky-like anomaly near 200 K [which would correspond to an energy splitting of approximately 45 meV if fit to a fixed $\Delta E(T)$] which originates from a competition between the nonmagnetic $S = 0$ ground state of the Rh atom and the ferromagnetic $S_{\text{Rh}} \parallel S_{\text{Fe}}$ alignment of the Rh moment; in the AFM state, $S = 0$ is the ground state, but the exchange interaction with Fe lowers the energy of the $S_{\text{Rh}} \parallel S_{\text{Fe}}$ state for the FM state, producing a two-state system in the FM which yields a Schottky-like heat capacity and entropy. This two-state system only occurs in the FM alloy because $J_{\text{Fe-Rh}}$ cancels at the Rh site in the AFM state due to the antiparallel alignment of the Fe spins. The additional entropy and enthalpy of this two-state system lowers the Gibbs free energy of the FM phase, finally matching that of the AFM phase at $T_{\text{AFM} \rightarrow \text{FM}}$, thus driving the transition.

A more recent model for magnetic entropy was put forth by Gu and Antropov [10], who suggest the transition is caused by the different magnon excitations of FM and AFM states. In their model, the magnon DOS in the FM state is much larger than that of the AFM state. This increased heat capacity causes a larger reduction in free energy with increasing T in the FM state than in the AFM state, causing the observed AFM to FM transition. In their calculation, the heat capacity of this magnon-driven model shows a peak difference between the two phases at about 300 K, significantly higher than what is observed experimentally (see Fig. 2) but of the same general temperature dependence.

The even more recent model of Sandratskii and Mavropoulos has a more sophisticated model for the

magnetization, particularly for the Rh moment in the AFM state, which possesses substantial local polarization despite having no net moment [11]; it is not clear how this would translate into heat capacity differences between the two competing phases of FeRh, but the entropy associated with the Rh moments in the AFM state clearly must play a significant role.

More generally, C_P of the FM state (as well as the excess C_P , which is dominated by $C_{P,FM}$) has a temperature dependence which is unusual, reflecting the complex magnetic properties seen in all the models for this system. While it is possible that a more accurate lattice C_P would modify this dependence, it is clear from all measurements (low-temperature specific heat, room temperature sound velocity, and shear modulus) that the FM state has a stiffer lattice than the AFM state, and it is therefore highly unlikely that the excess specific heat seen near 100 K is due to unusual lattice contributions for the FM state not seen in the AFM state. It is far more likely that the excess heat capacity is due to magnetic excitations, such as those discussed above or, more generally, as typically seen in itinerant ferromagnets with spin fluctuations that saturate at moderately high T (e.g., Refs. [29–31]).

Conclusions.—Specific heat measurements of epitaxial ferromagnetic $\text{Fe}_{1.04}\text{Rh}_{0.96}$ and antiferromagnetic $\text{Fe}_{0.98}\text{Rh}_{1.02}$ thin films show an excess magnetic specific heat of the FM sample, with a peak near 100 K corresponding to an energy splitting of 16 ± 1 meV when fit to a Schottky anomaly. The data indicate the importance of magnetic fluctuations in driving the AFM > FM transition, with the electronic contribution providing a smaller contribution and the lattice actually lowering the free energy of the AFM phase relative to the FM phase, hence resisting the transition. Though qualitatively the peak in heat capacity is consistent with existing magnetic fluctuation models of the transition, it occurs at a lower temperature than theoretically predicted and requires further theoretical input to understand the magnetic fluctuations in this complex magnetic system. Finally, from the integrated heat capacity of the two phases, we obtain an entropy difference $\Delta S_{FM-AFM} = 17 \pm 3$ J/kg/K (2.7 ± 0.5 J/mol/K) and a $T = 0$ energy difference of 3.4 J/g (540 J/mol), consistent with literature values of the latent heat of the transition and theoretical calculations of the two ground states.

We would like to thank Jean Juraszek for insight from Mössbauer spectrometry, David G. Cahill for his work on sound velocity measurements, Asif Khan for the high-temperature x-ray diffraction measurements, and Alex X. Gray and Charles S. Fadley for photoemission work and discussions. This project was supported by the Director of the Materials Sciences and Engineering Division, Office of Basic Energy Sciences, Office of Science, U.S. Department of Energy under Contract No. DE-AC02-05CH11231. Growth of the films at UCSD was supported under DOE-BES Award No. DE-SC0003678.

*dcooke@berkeley.edu

- [1] J.-U. Thiele, S. Maat, and E. E. Fullerton, *Appl. Phys. Lett.* **82**, 2859 (2003).
- [2] M. Fallot, *Ann. Phys. (Paris)* **10**, 291 (1938).
- [3] M. Richardson, D. Melville, and J. Ricodeau, *Phys. Lett.* **46A**, 153 (1973).
- [4] J. A. Ricodeau and D. Melville, *J. Phys. F* **2**, 337 (1972).
- [5] A. I. Zakharov *et al.*, *Sov. Phys. JETP* **19**, 1348 (1964).
- [6] P. Tu, A. J. Heeger, J. S. Kouvel, and J. B. Comly, *J. Appl. Phys.* **40**, 1368 (1969).
- [7] C. Koenig, *J. Phys. F* **12**, 1123 (1982).
- [8] B. Fogarassy, T. Kemény, L. Pál, and J. Tóth, *Phys. Rev. Lett.* **29**, 288 (1972).
- [9] M. E. Gruner, E. Hoffmann, and P. Entel, *Phys. Rev. B* **67**, 064415 (2003).
- [10] R. Y. Gu and V. P. Antropov, *Phys. Rev. B* **72**, 012403 (2005).
- [11] L. M. Sandratskii and P. Mavropoulos, *Phys. Rev. B* **83**, 174408 (2011).
- [12] S. O. Mariager *et al.*, *Phys. Rev. Lett.* **108**, 087201 (2012).
- [13] N. V. Kreiner, H. Michor, G. Hilscher, N. V. Baranov, and S. V. Zemlyanski, *J. Magn. Magn. Mater.* **177–181**, 581 (1998).
- [14] D. W. Cooke, F. Hellman, J. R. Groves, B. M. Clemens, S. Moyerman, and E. E. Fullerton, *Rev. Sci. Instrum.* **82**, 023908 (2011).
- [15] D. W. Cooke, Ph.D. thesis, University of California, 2010.
- [16] R. Bachmann *et al.*, *Rev. Sci. Instrum.* **43**, 205 (1972).
- [17] D. W. Denlinger, E. N. Abarra, K. Allen, P. W. Rooney, M. T. Messer, S. K. Watson, and F. Hellman, *Rev. Sci. Instrum.* **65**, 946 (1994).
- [18] D. R. Queen and F. Hellman, *Rev. Sci. Instrum.* **80**, 063901 (2009).
- [19] See Supplemental Material at <http://link.aps.org/supplemental/10.1103/PhysRevLett.109.255901> for high-temperature XRD above and below the transition.
- [20] Here we define a mole based on the CsCl unit cell (e.g., 1 mole $\text{Fe}_{0.98}\text{Rh}_{1.02}$ weighs 159.7 g).
- [21] T. Lee, K. Ohmori, C.-S. Shin, D. Cahill, I. Petrov, and J. Greene, *Phys. Rev. B* **71**, 144106 (2005).
- [22] A. I. Zakharov, *Fiz. Met. Metalloved.* **24**, 84 (1967).
- [23] W. Nernst and F. A. Lindemann, *Z. Elektrochem.* **17**, 817 (1911); A. P. Miller, *Cindas Data Series on Material Properties Specific Heat of Solids* (Hemisphere/CINDAS, New York, 1988), Vols. 1 and 2.
- [24] M. P. Annaorazov, K. A. Asatryan, G. Myalikgulyev, S. A. Nikitin, A. M. Tishin, and A. L. Tyurin, *Cryogenics* **32**, 867 (1992).
- [25] A. X. Gray *et al.*, *Phys. Rev. Lett.* **108**, 257208 (2012).
- [26] See Supplemental Material at <http://link.aps.org/supplemental/10.1103/PhysRevLett.109.255901> for the magnetic contributions to the entropy of the FM and AFM Fe-Rh alloys.
- [27] M. P. Annaorazov, S. A. Nikitin, A. L. Tyurin, K. A. Asatryan, and A. Kh. Dovletov, *J. Appl. Phys.* **79**, 1689 (1996).
- [28] J. Kouvel, *J. Appl. Phys.* **37**, 1257 (1966).
- [29] Y. Takahashi, T. Kanomata, R. Note, and T. Nakagawa, *J. Phys. Soc. Jpn.* **69**, 4018 (2000).
- [30] P. Mohn and G. Hilscher, *Phys. Rev. B* **40**, 9126 (1989).
- [31] Y. Takahashi, *J. Phys. Condens. Matter* **11**, 6439 (1999).